ADVANCED MATERIALS
www.advmat.de

Encrypted Thermal Printing with Regionalization Transformation

Run Hu, Shiyao Huang, Meng Wang, Xiaobing Luo, Junichiro Shiomi,* and Cheng-Wei Qiu**

Artificially structured thermal metamaterials provide an unprecedented possibility of molding heat flow that is drastically distinct from the conventional heat diffusion in naturally conductive materials. The Laplacian nature of heat conduction makes the transformation thermotics, as a design principle for thermal metadevices, compatible with transformation optics. Various functional thermal devices, such as thermal cloaks, concentrators, and rotators, have been successfully demonstrated. How far can it possible go beyond just realizing a heat-distribution function in a thermal metadevice? Herein, the concept of encrypted thermal printing is proposed and experimentally validated, which could conceal encrypted information under natural light and present static or dynamic messages in an infrared image. Regionalization transformation is developed for structuring thermal metamaterial-strokes as infrared signatures, enabling letters of the alphabet to be written, paintings to be drawn, movies to be made, and information to be displayed. This strategy successfully demonstrates an extreme level of manipulation of heat flow for encryption, illusions, and messaging.

Since the birth of transformation optics (TO) theory, a plethora of extraordinary phenomena and functionalities has been developed, with a series of successful extensions of counterpart theories and functionalities in electromagnetic, thermotics, acoustics, and dc electric and mechanic fields.[1–10] The essence of TO and counterpart theories lies in the form invariance of the governing equations under coordinate transformation from one space to another; however, this gives rise to stringent requirements of transformed material parameters with anisotropy, inhomogeneity, and even singularity. The naturally existing homogeneous materials usually fail to meet such severe requirements, thus the alternative artificial structured materials, *a.k.a.* metamaterials, are gaining popularity in recent decade.[11–13] Thermal metamaterials, as an important branch in the family of metamaterials, have attracted much attention owing to their prominent potential of heat flow manipulation. Based on thermal metamaterials, many novel thermal functionalities and metadevices have been proposed, such as thermal cloaking, concentrating, camouflage, reflection, refraction, diode, encoding, and computation.[14–43] The essence of all these thermal functionalities is to manipulate the heat distribution by changing the local temperature field without influencing the remaining part (outside the metadevices) to achieve desired performances. For instance, thermal cloaking is to manipulate the heat flow passing around central region and returning back to the original direction, which looks as if heat flux passes through a homogeneous plate. The objects sitting in the central region are concealed from the outside observers with an infrared (IR) camera, thus the corresponding device is called as thermal cloak, originated from the counterpart of the invisibility cloak in TO theory.[15,16] For another example, most thermal camouflage is to achieve the same temperature field outside the illusion device region.[25–27] It is perceived that only the same outside temperature is not enough for perfect thermal camouflage, therefore the concept of illusion thermotics is proposed to achieve misleading temperature distribution outside and inside the device simultaneously.[28] In recent years, these thermal functionalities have been frequently invoked though with different structures, materials, implementations, and applicability. Beyond realizing an existing heat-distribution function in a thermal metadevice, how far can we go on the way of heat flow manipulation? In this study, we develop the regionalization transformation method for designing thermal metamaterials to realize the heat signatures of the entire alphabet from A to Z letter by letter, based on

Prof. R. Hu, S. Y. Huang, Prof. X. B. Luo
State Key Laboratory of Coal Combustion
School of Energy and Power Engineering
Huazhong University of Science and Technology (HUST)
Wuhan 430074, China
E-mail: luoxb@hust.edu.cn
M. Wang, Prof. X. B. Luo
China-EU Institute for Clean and Renewable Energy
Huazhong University of Science and Technology
Wuhan 430074, China
Prof. J. Shiomi
Department of Mechanical Engineering
The University of Tokyo (UTOKYO)
7-3-1 Hongo, Bunkyo-ku, Tokyo 113-8656, Japan
E-mail: shiomi@photon.t.u-tokyo.ac.jp
Prof. C.-W. Qiu
Department of Electrical and Computer Engineering
National University of Singapore (NUS)
Kent Ridge 117583, Republic of Singapore
E-mail: eleqc@nus.edu.sg
The ORCID identification number(s) for the author(s) of this article can be found under https://doi.org/10.1002/adma.201807849.

DOI: 10.1002/adma.201807849

 © 2019 WILEY-VCH Verlag GmbH & Co. KGaA, Weinheim

which we propose the concept of thermal metamaterial-based encrypted thermal printing. Comparative discussions are presented to verify the advantages of the proposed metamaterials and the thermal printing concept. Other than printing the alphabet, more possibilities of the encrypted thermal printing are explored as well.

To start, we develop the regionalization transformation method as follows. The whole space, Ω, can be divided into several subspaces Ω_i (i = 1, 2, 3...) with $\Omega_i \cap_{i\neq j} \Omega_j = 0$. For easy implementation, the number of the subspaces should be as small an integer as possible. In each subspace Ω_i, we implement different linear coordinate transformations, $\Omega_i : \mathbf{x}_i = (x_i, y_i, z_i) \rightarrow \Omega'_{i'} : \mathbf{x}'_{i'} = (x'_{i'}, y'_{i'}, z'_{i'})$, depending on the desired shape of thermal illusions, and accordingly obtain the different thermal conductivity tensors $\kappa'(\mathbf{x}_i)$ based on the illusion thermotics.[28] Heat conduction in the original subspace Ω_i and the transformed subspace Ω_i' is governed as

$$\rho(\mathbf{x}_i)c(\mathbf{x}_i)\frac{\partial T_i}{\partial \tau} = \nabla\left(\kappa(\mathbf{x}_i)\cdot\nabla T_i\right) + Q_0 H(\tau)\delta(\mathbf{x}_i - \mathbf{x}_0) \quad (1)$$

$$\rho'(\mathbf{x}_i)c'(\mathbf{x}_i)\frac{\partial T'_i}{\partial \tau} = \nabla\left(\kappa'(\mathbf{x}'_i)\cdot\nabla T'_i\right) + Q_0 H(\tau)\delta(\mathbf{x}'_i - \mathbf{x}_0) \quad (2)$$

where ρ, c, and κ are the density, specific heat, and thermal conductivity, respectively. $H(\tau)$ is the Heaviside function to denote the turning on and constant working of heat source for $\tau > 0$. $\delta(\mathbf{x}_i - \mathbf{x}_0)$ is a delta function to denote the location of the heat source. Q_0 is the power of the heat source. From Equations (1) and (2), we can see that though the space coordinates are transformed, the location and the power of the heat source remain unchanged, which is consistent with our real implementation. The transformed $\kappa'(\mathbf{x}_i)$ in each subspace can be calculated from the transformation thermotics as $\kappa'(\mathbf{x}_i) = \frac{\mathbf{J}(\mathbf{x}_i)\kappa_0\mathbf{J}^T(\mathbf{x}_i)}{\det(\mathbf{J}(\mathbf{x}_i))}$,[4,5] where κ_0 is the homogeneous thermal conductivity of the virtual space and $\mathbf{J}$ is the Jacobian matrix of the coordinate transformation as $\mathbf{J}(\mathbf{x}_i) = \partial(\mathbf{x}'_i)/\partial(\mathbf{x}_i)$. In general, as shown in **Figure 1**a, we move the illusion target ($PQMN$) in the virtual space (x, y) to the real target ($P'Q'M'N'$) in the real space (x', y'). The regions of $ABCD$ or $A'B'C'D'$ are the illusion device region. The location, shape, and rotation angle θ of the illusion target can be tuned in terms of the real target. Both the virtual and real spaces are divided into some triangles. The real target is located at one corner here, so there are only four triangular regions of interest (denoted by 1′, 2′, 3′, and 4′). Since the coordinates of the illusion targets ($PQMN$) can be adjusted, we can realize moving, shaping, rotating, and splitting functions as desired. More details can be found in our previous paper.[28] We then use a linear coordinate transformation to map the points in each triangular region for the sake of experimental feasibility. With the transformed $\kappa'(\mathbf{x}_i)$, we can manufacture the samples in each subspace. Then setting the origin in each subspace as an independent heat source, heat conducts separately along the designed direction between the original and virtual illusions to achieve one stroke and the resulting heat signatures make up the complete infrared picture of the desired letters. It is perceived that the temperature continuity will not be satisfied at the boundaries of adjacent subspaces, i.e., $T_i|_{d\Omega_i} \neq T_j|_{d\Omega_j}$ and $\frac{\partial T_i}{\partial \mathbf{x}_i}\Big|_{d\Omega_i} \neq \frac{\partial T_j}{\partial \mathbf{x}_j}\Big|_{d\Omega_i}$. However, such boundary discontinuity makes little difference to the final infrared signatures of the letters due to the gap between each pair of subspaces. Note that the dimension and power of the heat source in each subspace are not confined; in general and for simplification, they are consistent in our following design.

According to the stroke characteristics, the alphabet can be sorted into three groups as follows if we set the center point as the origin: in Group 1, letters such as "I," "J," "K," "L," "T,"

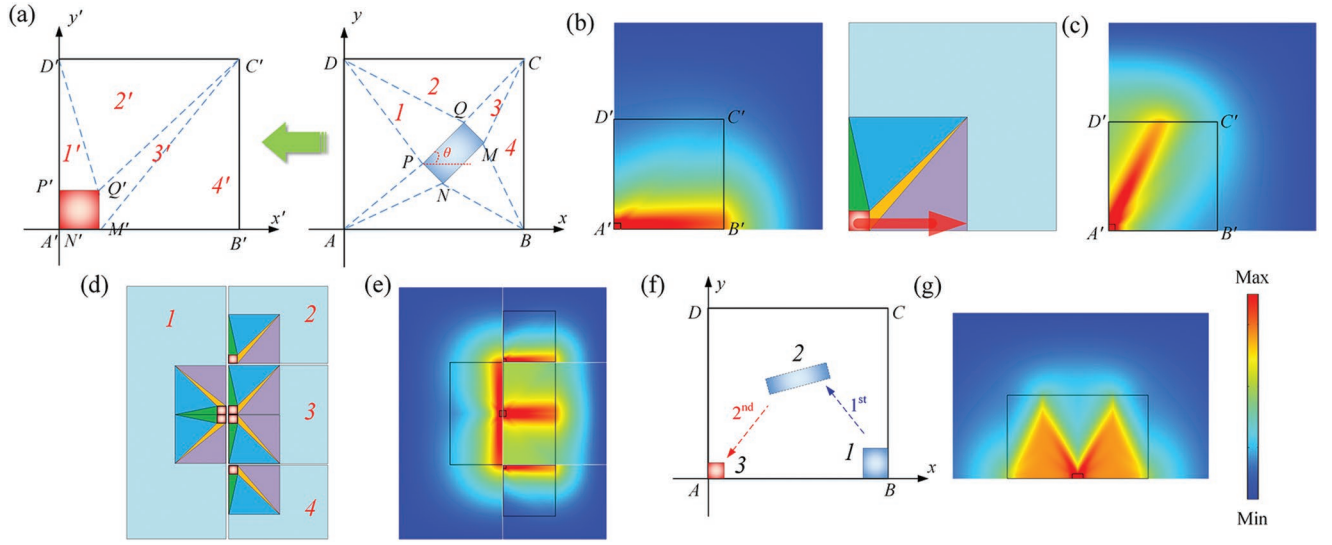

Figure 1. Schematics of the regionalization transformation. a) Schematic of the general coordinate transformation in illusion thermotics. The rectangle $PQMN$ with rotation angle of θ in the virtual space is moved to the rectangle $P'Q'M'N'$ in the real space. b) Heat signatures of one basic stroke and the corresponding basic building block. Four rectangular regions in different colors denote different thermal conductivity tensors in Table 1. The red arrow shows that heat, rather than the omnidirectional diffusion, conducts along the purple triangular region boundary. c) Heat signatures of another basic stroke, in which heat conducts along the blue triangular region. The corresponding building block is of the same dimension as that in (b) except for the different thermal conductivity tensors in each triangular region. d) Schematic of regionalization transformation composed by the basic building block in (b), and e) the heat signature of the letter "E." f) Schematic of the double transformation and g) the heat signature of the letter "M."

© 2019 WILEY-VCH Verlag GmbH & Co. KGaA, Weinheim

"V," "X," and "Y" that have only one straight stroke in each quadrant; in Group 2, letters such as "M," "N," "W," and "Z" that possess multiple strokes in one quadrant and the stroke-folding angle is nonorthogonal; in Group 3, the remaining letters that possess multiple straight strokes in each quadrant, but their stroke-folding angles are orthogonal. Due to the multiple-stroke characteristics of some letters, only one heat source in the origin is not sufficient to achieve the infrared signatures of the letters clearly, and at least two basic transformations are needed. As shown in Figure 1b, the illusion target is located at $P(20, 5)$ mm with dimensions of $PQ = 25$ mm and $PN = 2$ mm without rotation. The dimensions of the illusion device and the real target are 50 mm × 50 mm and 5 mm × 5 mm, respectively. The boundary lines $A'B'$ and $A'D'$ are kept adiabatic while the other two are cooled by natural convection at room temperature. The volumetric power of the heat source (real target $P'Q'M'N'$) is 10 Watts. As claimed in our previous study,[28] the region *1′* in Figure 1a is responsible for the thermal camouflage outside the device and the region *4′* is responsible for the splitting function inside the device. Since we do not need the thermal camouflage outside the device in this study, we exchange the κ_x and κ_y just for the region *1′*. Such a coordinate transformation results in an overlap of the heat signature with boundary $A'B'$ (Figure 1b). To design the building block, we use four different colors to represent the four triangular regions with different thermal conductivity tensors tabulated in **Table 1**. When the heat source is turned on, heat conducts along purple triangular boundary rather than omnidirectional diffusion. Such a heat signature could act as one basic stroke, which is frequently used in the following designs. As shown in Figure 1c, the illusion target is located at $P(20, 25)$ mm with dimensions of $PQ = 25$ mm and $PN = 2$ mm without rotation and other conditions are kept the same. The resulting heat signature is shown in Figure 1c, where heat conducts along the blue triangular region. The corresponding building block possesses the same dimension and structure as that for Figure 1b, except for the different thermal conductivity tensors. The shape and size of the stroke can be further adjusted by changing the coordinates of the illusion target.

To achieve the heat signature of the entire alphabet, we next apply the proposed regionalization transformation method to design thermal metamaterials letter by letter based on the two basic strokes in Figure 1b,c. Taking the letter "E" as an example (Figure 1d,e), we divide the whole space into four subspaces (subspaces 1, 2, 3, and 4). The four subspaces are not in contact with each other, and that is the reason why there are white gaps in Figure 1d,e. All the outside boundaries are cooled at natural convection and the adjacent boundaries of the four subspaces are adiabatic. Each region possesses an independent transformation to realize the heat signatures in Figure 1b, and the corresponding signature in each region plays the role of one stroke. With proper design, the desired signature of letter "E" is realized in Figure 1e. Note that the strokes are orthogonal in the letter "E," and thus the letters in Group 3 can be realized only based on the basic stroke in Figure 1b. In fact, all the letters can be achieved by this regionalization transformation method, but due to symmetry, the letters in Groups 1 and 2 can be realized in a simpler way. For Group 1, the letters can be realized by the previous general illusion thermotics method. For instance, we have realized the heat signature of letter "X" in our previous study with experimental verification.[28] We can also use the symmetric treatment of Figure 1b,c to realize the heat signatures of these letters. Since the dividing regions are not in contact with each other in the regionalization transformation, the mutual influence of any two regions can be eliminated, resulting in clearer strokes. Therefore, we choose the regionalization transformation to realize the letters "J," "K," "L," "T," and "Y" for clearer demonstration. For Group 2, we propose the double-transformation method. As shown in Figure 1f, a coordinate transformation is first used to move the target from position 1 to position 2, and then another is used to move the target from position 2 to position 3. Using such double transformation, we can realize the heat signature of letters "M," "N," "W," and "Z," respectively. The "M" signature can be seen in Figure 1g. It is seen that because there is only one heat source, the temperature decreases gradually along the designed direction/paths, thus the contour of the letter "M" became fuzzy in the downstream.

Table 1. Transformed thermal conductivity tensors in each triangular region in the real space in Figure 1b.

	1′	2′	3′	4′
κ'[a)]	$\begin{bmatrix} 8.704 & 0.444 \\ 0.444 & 0.138 \end{bmatrix}$	$\begin{bmatrix} 1.791 & 0.933 \\ 0.933 & 1.044 \end{bmatrix}$	$\begin{bmatrix} 6.267 & -2.733 \\ -2.733 & 1.352 \end{bmatrix}$	$\begin{bmatrix} 9.400 & 0.600 \\ 0.600 & 0.145 \end{bmatrix}$
$\kappa'_{x,y}$	$\begin{bmatrix} 8.7555 & 0 \\ 0 & 0.0865 \end{bmatrix}$	$\begin{bmatrix} 2.4531 & 0 \\ 0 & 0.3819 \end{bmatrix}$	$\begin{bmatrix} 5.6278 & 0 \\ 0 & 1.9912 \end{bmatrix}$	$\begin{bmatrix} 9.4644 & 0 \\ 0 & 0.0806 \end{bmatrix}$
κ_A[a)]	17.396	4.631	14.903	18.824
κ_B[a)]	0.057	0.216	0.067	0.053
θ	−3.0°	34.1°	−24.0°	3.7°
f	0.207	0.804	0.32	0.142
η	3.83	0.24	2.125	6.037

[a)]Unit: W m^{-1} K^{-1}.

© 2019 WILEY-VCH Verlag GmbH & Co. KGaA, Weinheim

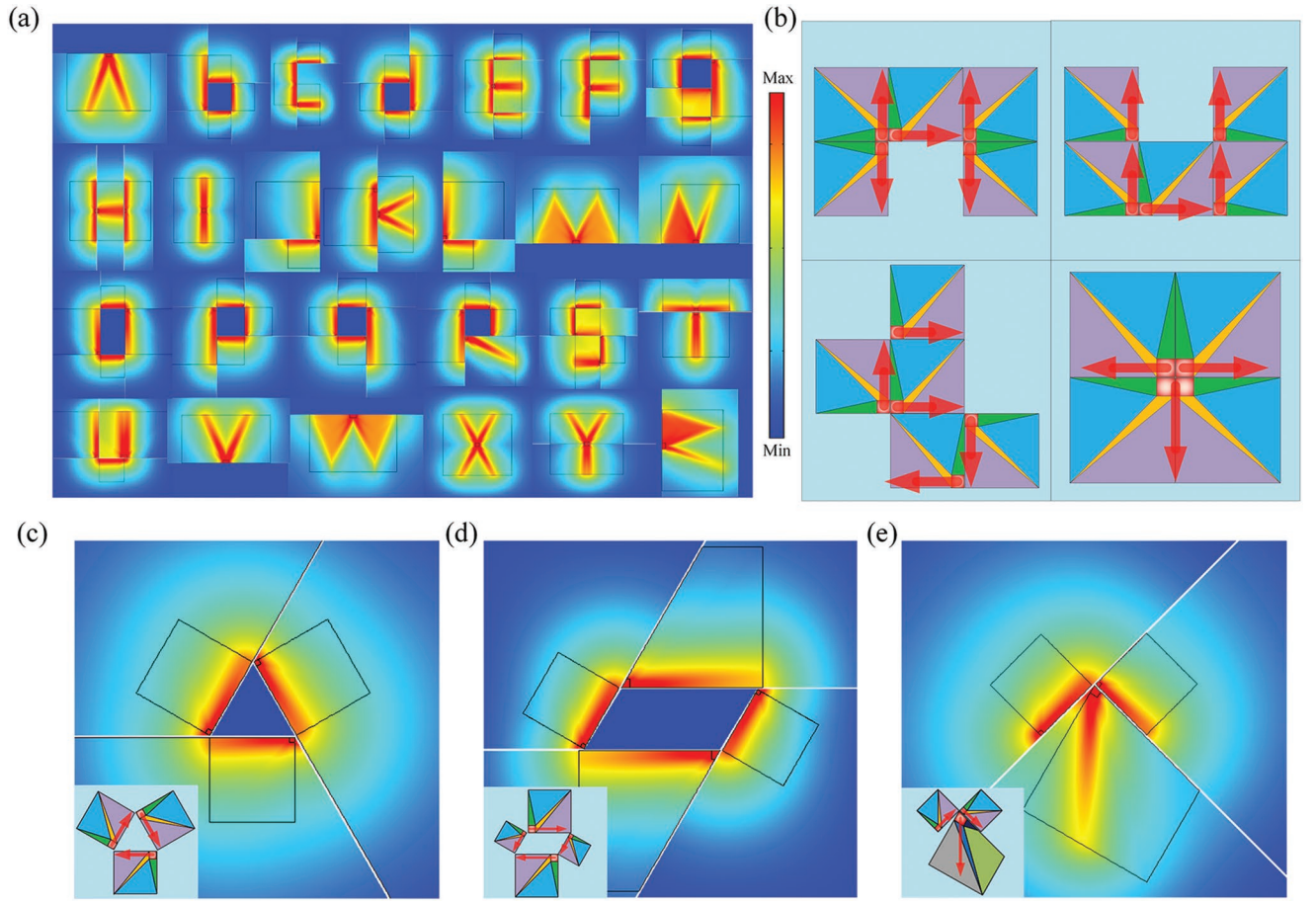

Figure 2. Thermal printing for alphabet and paintings through FEM simulations. a) Heat signatures of the entire alphabet and b) schematic of regionalization transformation composed by the basic building block in Figure 1b to denote the abbreviation "HUST". The red arrows denote the heat conduction direction along the purple triangular region. Most letters in the entire alphabet are achieved by the regionalization transformation method, and some are achieved by general illusion thermotics and double-transformation method. c–e) Heat signatures of a triangle (c), a parallelogram (d), and an arrow (e), and the insets in each subfigure show the regionalization design of basic building blocks.

With the above design methods, we can realize the entire alphabet as shown in **Figure 2**a through finite-element method (FEM) simulations. Taking the letters "H," "U," "S," and "T" as examples in Figure 2b, we show the corresponding assembly of the basic building blocks of Figure 1b. As the red arrows show, heat conducts along the purple triangle boundary, and the resulting heat signatures achieve the designed letters clearly. Similarly, we can also "write" numbers from 0 to 9 or even "draw" paintings using such infrared strokes as the brush. Figure 2c–e demonstrates the thermal paintings of a triangle, a parallelogram, and an arrow with proper space regionalization. Inspired by the thermal paintings, we are more confident in achieving the heat signatures of the letters in Group 2 by the regionalization transformation method. Moreover, by extending to a three-dimensional space or splitting the target into several parts in one quadrant, more possibilities and more degrees of freedoms become available.

One may wonder why not to design a structure with the same shape as the desired letters using homogenous materials. To figure out the difference, we design a structure with the shape of letter "T" and compare the heat signature on the homogenous material with that on the proposed thermal metamaterials. To realize the transformed thermal conductivity tensor κ' of the thermal metamaterials, we first diagonalize the κ' into $\mathrm{diag}(\kappa'_x, \kappa'_y)$, where $\kappa'_{x,y} = \left(\kappa'_{xx} + \kappa'_{yy} \pm \sqrt{(\kappa'_{xx} - \kappa'_{yy})^2 + 4\kappa'^2_{xy}}\right)/2$, and the rotation angle θ is $\theta = 0.5\tan^{-1}[2\kappa'_{xy}/(\kappa'_{xx} - \kappa'_{yy})]$. Then, according to effective medium approximation (EMA) theory, we try to realize $\mathrm{diag}(\kappa'_x, \kappa'_y)$ on the two rotated layered homogeneous materials A and B with $\kappa_{A,B} = \kappa'_x \pm \sqrt{\kappa'^2_x - \kappa'_x \kappa'_y}$ when the layer thickness is uniform.[28,29] The calculated κ_A, κ_B, and θ are also listed in Table 1. It is difficult to tell what exactly the letter is based on the temperature contours in **Figure 3**a, but the temperature contours in Figure 3b clearly show the letter "T." Moreover, when the heat source is not working, the letter "T" in the subfigure of Figure 3a is still observable from the material difference with the naked eyes, but it is completely camouflaged using the proposed thermal metamaterials in Figure 3c. As for the experiments, we drilled invar steel with paralleled stripes and holes. The effective thermal conductivity tensor is $\mathrm{diag}(\kappa_{x'}, \kappa_{y'})$, where $\kappa_{x'} = f\kappa_{\mathrm{air}} + (1-f)\kappa_{\mathrm{steel}}$ and $\kappa_{y'} = (f/\kappa_{\mathrm{air}} + (1-f)/\kappa_{\mathrm{steel}})^{-1}$ with f and κ_{air} being the filling ratio and the thermal conductivity of the stripes/holes (air), respectively. By making the calculated thermal conductivity tensors equivalent to the experimental

© 2019 WILEY-VCH Verlag GmbH & Co. KGaA, Weinheim

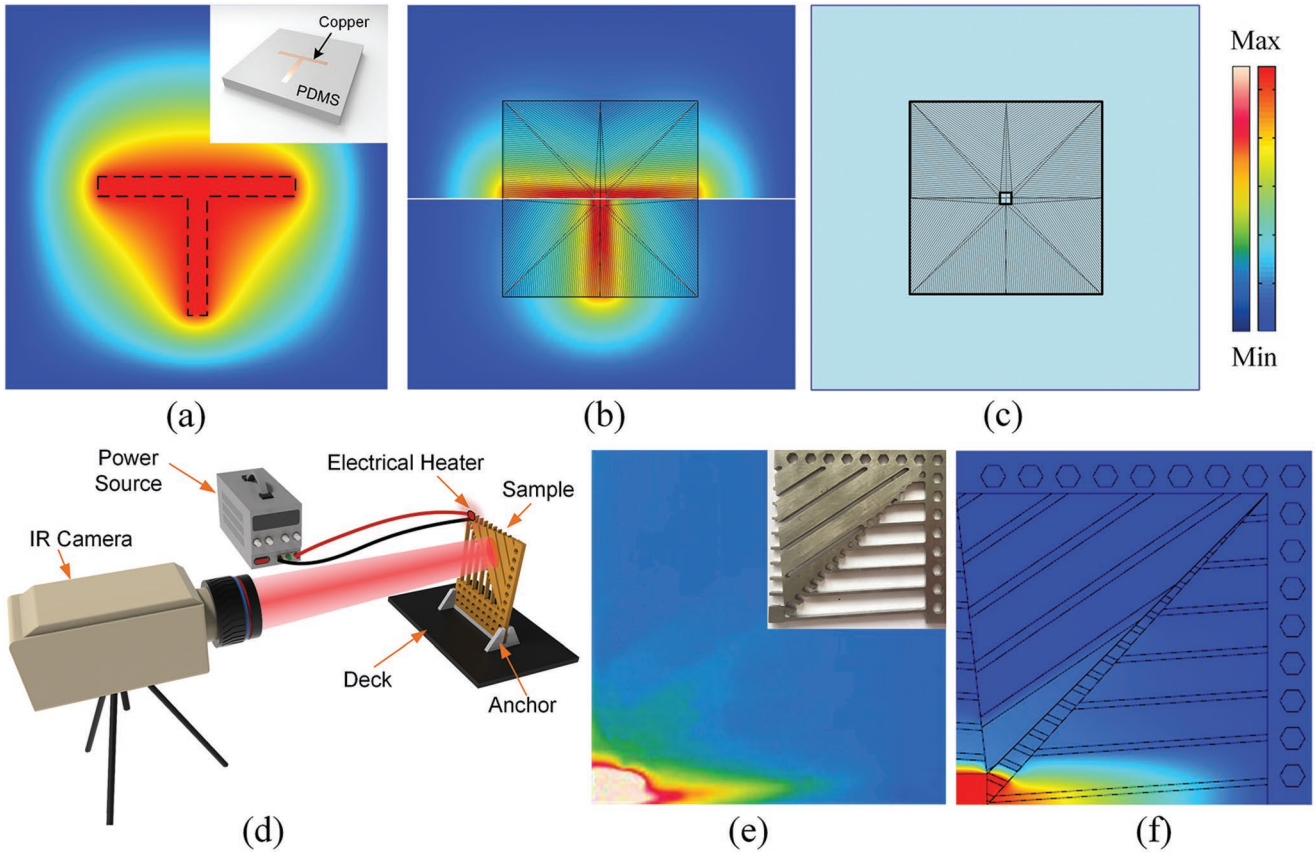

Figure 3. Validating the advantages of the proposed thermal metamaterials in simulation and experiment. a) Temperature field of a polydimethylsiloxane (PDMS) homogenous plate with imbedding copper "T"-shape structure. The inset shows the simulation setup in the visible light spectrum, thus we can see the letter "T" clearly. b) Temperature field of the proposed thermal metamaterials to display the heat signature of letter "T." c) The layout of the corresponding metamaterials, which are composed by two kinds of layered homogeneous materials of A and B with different homogeneous thermal conductivity tensors tabulated in Table 1 and a uniform layer thickness of 1 mm. Compared to that in (a), the letter "T" realized by the proposed thermal metamaterials is encrypted under natural light, while it is printed in the infrared image after turning on the heat source. d) Experimental setup schematic. e) Experimental and f) simulated temperature fields with layered structures to consistently show heat conduction along specific direction rather than omnidirectional diffusion, validating the feasibility of basic stroke in Figure 1b. The inset in (e) shows the experimental sample made by invar steel with drilled holes.

ones ($\mathrm{diag}(\kappa'_x,\kappa'_y) \approx \mathrm{diag}(\kappa_{x'},\kappa_{y'})$), we obtained the filling ratio f and the layer thickness ratio $\eta = t_{\mathrm{air}}/t_{\mathrm{steel}}$ in each triangular region in the device, as listed in Table 1. Figure 3d shows the experimental setup and more details of the experimental fabrication and process can be found in Section S1 (Supporting Information). In addition to experiments, FEM simulations were also performed for the devices with the same dimensions, materials, and boundary conditions as the experiments. The experimental and simulated results are shown in Figure 3e,f; the results agree well with each other in terms of temperature distribution. The experimental prototype is shown in the inset of Figure 3e. Heat is conducted horizontally along one boundary rather than omnidirectional diffusion, validating the design purpose for extreme heat manipulation. Though not perfect, heat is still successfully manipulated to conduct along one direction and realize the basic "thermal stroke" experimentally as depicted in Figure 1b. The discrepancy between the experimental and simulation results can be explained as follows. First, the experimental thermal conductivity tensor is not as anisotropic as that in theory. Since we preset the two materials as invar steel and air, the filling ratio f is not always solvable so that κ_B can approximate, but may not be completely equal to, the thermal conductivity of air. Second, the thickness of the two materials should be as thin as possible to make the EMA more accurate. But in the real fabrication, the minimum thickness of t_{air} is 3 mm, which is larger than the thickness in Figure 3b,c. Third, in region *2′* the required filling ratio f is rather small, while in region *4′* the required f is rather large, resulting in quite few alternative layers there. Thus, the effective thermal conductivities are not as accurate as those designed by EMA. Fourth, air convection and interfacial thermal resistance are ignored in the 2D simulation but exist in experiments. Effort may be made in the aforementioned four aspects to improve the experimental demonstration, like fabricating larger samples to improve the accuracy of EMA with more alternative layers, using 3D printing to manufacture the samples with decreased minimum thickness, etc.

What can we do with the proposed thermal metamaterials? Here, we show one possibility to display the information based

© 2019 WILEY-VCH Verlag GmbH & Co. KGaA, Weinheim

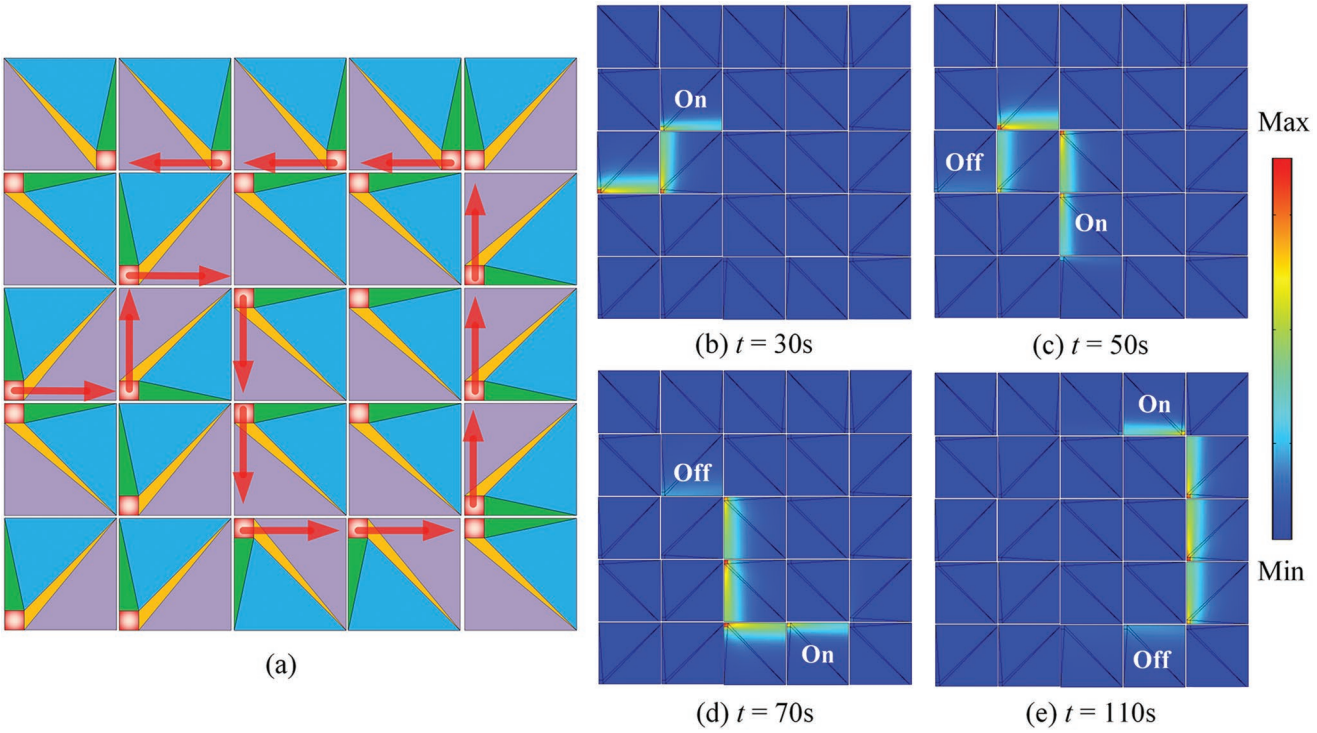

Figure 4. Thermal printing for "Gluttonous Snake." a) Assembly setup of an array of the 5 × 5 basic building blocks in Figure 1b and the red arrows represent the direction of heat flow in each block. The heat source in each block will be turned on/off according to the preset design sequence with a time delay of 10 s. Snapshots of the thermal movie with "Gluttonous Snake" at b) 30 s, c) 50 s, d) 70 s, and e) 110 s. Before t = 40 s, the Gluttonous snake elongates itself, and maintains its length afterward by turning off the last heat source at every 10 s interval.

on the infrared alphabet or paintings. We realize the heat signatures of the abbreviations of "HUST," "UTOKYO," and "NUS"; readers may access a short video of the transient demonstration of the infrared signatures in Section S2 (Supporting Information). The information encrypted on the plate is not clear in the beginning (when heat sources are not working), and after turning on the heat sources, the heat signatures gradually show what we want to display. We could also control the switching on/off of the heat sources to make a thermal movie. An interesting demonstration of the classical computer game called as "Gluttonous Snake" is shown in **Figure 4**, and the transient movie is shown in Section S3 (Supporting Information). Based on such kind of switch on/off scheme, it is perceived that more complicated thermal paintings or movies can be realized. Since the present extreme manipulation is developed from the general illusion thermotics,[28] we may find more practical applications of thermal illusions and camouflages based on the proposed thermal metamaterials, like shrinking/magnifying thermal illusions, reshaping virtual heat sources, etc.

In summary, we proposed and experimentally validated the concept of encrypted thermal printing by developing the regionalization transformation method to design thermal metamaterials. Based on the proposed method, we realized the infrared signatures of the entire alphabet letter by letter according to the stroke characteristics of the alphabet. We also used the infrared strokes as brush for thermal paintings and thermal movies based on the switch on/off scheme. The advantages of the proposed thermal printing are verified with homogenous materials, i.e., the information can be encrypted under natural light and can be printed in the infrared image. The proposed thermal encrypted printing is more like a piece of paper or an infrared monitor, on which we can write letters, draw paintings, make movies, and display information. This strategy successfully demonstrates an extreme level of manipulating heat flow for encryption, illusion, and messaging.

Supporting Information

Supporting Information is available from the Wiley Online Library or from the author.

Acknowledgements

The authors acknowledge the financial support from the National Natural Science Foundation of China (Grant Nos. 51606074 and 51625601), the Ministry of Science and Technology of the People's Republic of China (Project No. 2017YFE0100600), and the National Key Research and Development Program of China (Project No. 2016YFB0400804). C.-W.Q. acknowledges the financial support from the Ministry of Education, Singapore (Project No. R-263- 000-C05-112).

Conflict of Interest

The authors declare no conflict of interest.

© 2019 WILEY-VCH Verlag GmbH & Co. KGaA, Weinheim

Keywords

illusion thermotics, regionalization transformation, thermal metamaterials, thermal printing

Received: December 5, 2018
Revised: April 5, 2019
Published online: May 6, 2019

[1] J. B. Pendry, D. Schurig, D. R. Smith, *Science* **2006**, *312*, 1780.
[2] U. Leonhardt, *Science* **2006**, *312*, 1777.
[3] D. Schurig, J. J. Mock, B. J. Justice, S. A. Cummer, J. B. Pendry, A. F. Starr, D. R. Smith, *Science* **2006**, *314*, 977.
[4] C. Z. Fan, Y. Gao, J. P. Huang, *Appl. Phys. Lett.* **2008**, *92*, 251907.
[5] S. Guenneau, C. Amra, D. Veynante, *Opt. Express* **2012**, *20*, 8207.
[6] K. H. Matlack, M. S. Garcia, A. Palermo, S. D. Huber, C. Daraio, *Nat. Mater.* **2018**, *17*, 323.
[7] J. Li, L. Fok, X. Yin, G. Bartal, X. Zhang, *Nat. Mater.* **2009**, *8*, 931.
[8] Y. G. Ma, Y. C. Liu, M. Raza, Y. D. Wang, S. L. He, *Phys. Rev. Lett.* **2014**, *113*, 205501.
[9] M. Moccia, G. Castaldi, S. Savo, Y. Sato, V. Galdi, *Phys. Rev. X* **2014**, *4*, 021025.
[10] T. Buckmann, M. Thiel, M. Kadic, R. Schittny, M. Wegener, *Nat. Commun.* **2014**, *5*, 4130.
[11] N. I. Zhuludev, Y. S. Kivshar, *Nat. Mater.* **2012**, *11*, 917.
[12] M. Maldovan, *Nature* **2013**, *503*, 209.
[13] S. A. Cummer, J. Christensen, A. Alu, *Nat. Rev. Mater.* **2016**, *1*, 16001.
[14] S. Narayana, Y. Sato, *Phys. Rev. Lett.* **2012**, *108*, 214303.
[15] R. Schittny, M. Kadic, S. Guenneau, M. Wegener, *Phys. Rev. Lett.* **2013**, *110*, 195901.
[16] H. Y. Xu, X. H. Shi, F. Gao, H. D. Sun, B. L. Zhang, *Phys. Rev. Lett.* **2014**, *112*, 054301.
[17] Y. M. Zhang, H. Y. Xu, B. L. Zhang, *AIP Adv.* **2015**, *5*, 053402.
[18] R. Hu, B. Xie, J. Y. Hu, Q. Chen, X. B. Luo, *Europhys. Lett.* **2015**, *111*, 54003.
[19] Y. G. Ma, L. Lan, W. Jiang, F. Sun, S. L. He, *NPG Asia Mater.* **2013**, *5*, e73.
[20] E. M. Dede, T. Nomura, P. Schmalenberg, J. S. Lee, *Appl. Phys. Lett.* **2013**, *103*, 063501.
[21] R. Hu, X. L. Wei, J. Y. Hu, X. B. Luo, *Sci. Rep.* **2015**, *4*, 3600.
[22] R. Hu, S. Y. Huang, M. Wang, L. L. Zhou, X. Y. Peng, X. B. Luo, *Phys. Rev. Appl.* **2018**, *10*, 054032.
[23] S. L. Zhou, R. Hu, X. B. Luo, *Int. J. Heat Mass Transfer* **2018**, *127*, 607.
[24] X. He, L. Z. Wu, *Appl. Phys. Lett.* **2014**, *105*, 221904.
[25] T. C. Han, X. Bai, J. T. L. Thong, B. W. Li, C. W. Qiu, *Adv. Mater.* **2014**, *26*, 1731.
[26] Y. R. Qiu, Q. Li, L. Cai, M. Y. Pan, P. Ghosh, K. K. Du, M. Qiu, *Light: Sci. Appl.* **2018**, *7*, 26.
[27] Q. W. Hou, X. P. Zhao, T. Meng, C. L. Liu, *Appl. Phys. Lett.* **2016**, *109*, 103506.
[28] R. Hu, S. L. Zhou, Y. Li, D. Y. Lei, X. B. Luo, C. W. Qiu, *Adv. Mater.* **2018**, *30*, 1707237.
[29] R. Hu, S. L. Zhou, W. C. Shu, B. Xie, Y. P. Ma, X. B. Luo, *AIP Adv.* **2016**, *6*, 125111.
[30] X. Y. Shen, C. R. Jiang, Y. Li, J. P. Huang, *Appl. Phys. Lett.* **2016**, *109*, 201906.
[31] Y. C. Liu, F. Sun, S. L. He, *Opt. Express* **2016**, *24*, 5683.
[32] Y. Kang, F. Yang, J. J. Urban, *Phys. Rev. Appl.* **2018**, *10*, 024034.
[33] A. Fiorino, D. Thompson, L. Zhu, R. Mittapally, S. A. Biehs, D. Bezencenet, N. E. Bondry, S. Bansropun, P. B. Abdallah, E. Meyhofer, P. Reddy, *ACS Nano* **2018**, *12*, 5774.
[34] A. L. Cottrill, S. Wang, A. T. X. Liu, W. J. Wang, M. S. Strano, *Adv. Energy Mater.* **2018**, *8*, 1702692.
[35] Y. Wang, A. Vallabhaneni, J. Hu, B. Qiu, Y. Chen, X. L. Ruan, *Nano Lett.* **2014**, *14*, 592.
[36] Y. Li, X. Y. Shen, Z. H. Wu, J. Y. Huang, Y. X. Chen, Y. S. Ni, J. P. Huang, *Phys. Rev. Lett.* **2015**, *115*, 195503.
[37] X. Y. Shen, Y. Li, C. R. Jiang, J. P. Huang, *Phys. Rev. Lett.* **2016**, *117*, 055501.
[38] L. Wang, B. W. Li, *Phys. Rev. Lett.* **2008**, *101*, 267203.
[39] F. Paolucci, G. Marchegiani, E. Strambini, F. Giazotto, *Phys. Rev. Appl.* **2018**, *10*, 024003.
[40] L. L. Zhou, S. Y. Huang, M. Wang, R. Hu, X. B. Luo, *Phys. Lett. A* **2019**, *383*, 759.
[41] S. R. Sklan, B. W. Li, *Natl. Sci. Rev.* **2018**, *5*, 138.
[42] K. P. Vemuri, F. M. Canbazoglu, P. R. Bandaru, *Appl. Phys. Lett.* **2014**, *105*, 193904.
[43] F. M. Canbazoglu, K. P. Vemuri, P. R. Bandaru, *Appl. Phys. Lett.* **2015**, *106*, 143904.

© 2019 WILEY-VCH Verlag GmbH & Co. KGaA, Weinheim